Preprint PFC/JA-84-40

HIGH BRIGHTNESS ELECTROSTATICALLY FOCUSSED FIELD EMISSION ELECTRON GUN FOR FREE ELECTRON LASER APPLICATIONS

D.A. Kirkpatrick, R.E. Shefer and G. Bekefi

Plasma Fusion Center and
Research Laboratory of Electronics
Massachusetts Institute of Technology
Cambridge, MA. 02139

October 1984

HIGH BRIGHTNESS ELECTROSTATICALLY FOCUSSED FIELD EMISSION ELECTRON GUN FOR FREE ELECTRON LASER APPLICATIONS

D.A. Kirkpatrick, R.E. Shefer and G. Bekefi

Department of Physics and Research Laboratory of Electronics

Massachusetts Institute of Technology

Cambridge Massachusetts 02139

ABSTRACT

An electrostatically focussed, multi-stage electron gun using a cold (field emission) cathode has been developed for use in a free electron laser. This gun produces a 1.1 kA, 2.0 MV electron beam with a normalized emittance $\epsilon_n \simeq 38 \times 10^{-3}$ (π-cm-rad), and a brightness of 74 kA/cm^{2}rad^2. The measured brightness is almost two orders of magnitude higher than that found in most RF linacs, and is comparable to that achieved using electron guns immersed in strong guiding magnetic fields. The emittance and brightness have been studied as a function of cathode material, surface finish and the electric field strength at the cathode surface.

I. INTRODUCTION

Relativistic electron beams with high current densities and low temperatures are a prerequisite for the successful operation of free electron lasers[1](FEL's) and other sources of coherent radiation employing electron beams. If high radiation powers are also a requirement, high currents in addition to high current densities are necessary. These requirements[2] become more and more stringent the shorter the radiation wavelength.

Beam brightness[3] is a useful measure of beam quality. Previous experimental studies[4-7] and numerical simulations[8] have shown that electron guns with cold (field emission) cathodes can attain high brightness. Unfortunately, these guns had to be immersed in strong guiding magnetic fields ranging from 10 kG to 90 kG. Moreover, as much as 90% of the "hot" outer regions of the beam had to be scraped off thereby dramatically reducing the overall FEL efficiency.

In this paper we will show that high beam brightness can be achieved from a cold cathode field emission gun in the complete absence of a guiding magnetic field. We shall describe the operation of an electrostatically focussed, multi-stage field emission electron gun[9] which produces a 1.1 kA, 2.0 MV electron beam with a normalized emittance $\epsilon_n \simeq 38 \times 10^{-3}$ (π-cm-rad) and a brightness of 74 kA/cm^{2}rad^2. Its characteristics are comparable to or exceed those achieved by other experimenters using electron guns immersed in strong guiding magnetic fields. The gun consists of a planar cathode and anode grid, followed by four accelerating stages. The accelerating electrodes are shaped[10] to provide electrostatic

focussing and obviate the need for any external magnetic field in the gun region. With several accelerating electrodes rather than just one, the electric field strength at the cathode surface can be reduced sufficiently in order to minimize electron emission from unwanted surfaces(see below). Such extraneous emission spoils the beam quality.

In section II we describe our electron gun and the experimental arrangement used in measuring the beam current, beam profile, and beam emittance. In section III we discuss the results and in section IV we compare our observations with those of other workers.

II. EXPERIMENTAL ARRANGEMENT

The experimental setup is shown in Fig. 1. A Physics International Pulserad 110 A electron accelerator (0.6 – 2.5 MV, 30 kA, 20 ns) is used to energize a five-stage multi-electrode field emission electron gun shown in Fig. 2. The electron beam is generated in the gap between the cathode and first anode (A1) by field emission from an emitting surface embedded in the cathode. The aperture of the first anode (A1) is covered with an 80% optically transmitting molybdenum mesh. The resultant beam is then accelerated to the full voltage by stages two through five. The aperture in the last anode (A5) is also covered with an 80% optically transmitting molybdenum mesh.

The cathode plate is a spin-formed aluminum disk with a cylindrical hole in the center, allowing the insertion of a plug of emitting material. The entire surface of the cathode, with the exception of the small emitting area, is anodized to minimize undesired emission.

The hard aluminum oxide (anodized) coating has a thickness of 0.05 mm. The cathode is mounted on a stalk which is adjustable in the axial direction allowing us to vary the cathode to first anode gap spacing. Different emitting materials are studied by removing and changing the plug of emitting material.

The voltages on the successive anodes A1 to A4 are $[-\frac{3}{4}V_0, -\frac{1}{2}V_0, -\frac{1}{4}V_0, -\frac{1}{8}V_0]$, where V_0 is the full accelerator voltage. For a 2 MV beam, for example, the successive voltages in megavolts from the cathode to the last anode are $[-2, -1.5, -1.0, -0.5, -0.25, 0]$. This division is achieved by means of an axisymmetric, cylindrical copper sulfate voltage divider (see Fig. 2) with which the electrodes are in electrical contact. Typically, the total resistance of this divider equals 400Ω. The shapes of the electrodes are designed[10] with the view of balancing the self electric and self magnetic fields of the beam so as to produce a paraxial electron beam of radius $r \simeq 2.5$ cm.

A calibrated Rogowski coil mounted at the beam exit is used to measure the transmitted electron current. The beam voltage is obtained by means of a voltage divider placed between the fourth and last(grounded) anodes. Typical voltage and current pulse traces are shown in Fig. 3. The current density profile $J(r)$, which is required in determining the beam emittance, is measured by placing a series of concentric circular apertures after the mesh in the last anode, and observing the transmitted current as measured by the Rogowski coil at the beam exit as a function of aperture radius.

The emittance is measured[3,11] by allowing the electron beam to impinge on an array

of 25 pinhole apertures in a 1.0 mm thick tantalum disk which takes the place of the mesh in the last anode. The apertures, each 0.5 mm in diameter, are separated by a distance of 0.7 cm in a 5×5 square pattern.

The transmitted beamlets are then allowed to traverse a field free region 24.0 cm in length before they strike a thin (0.4 mm) aluminum target which is coated on the downstream side with ZnS scintillator (see Fig. 1). The illumination pattern is photographed via a large (20 cm $\times$ 20 cm) mirror by a 35mm camera. The camera is shielded with concrete blocks. These and the mirror allow us to photograph the scintillator screen during the shot, while keeping the film from being exposed by x-rays generated by electrons hitting the aperture plate and the aluminum target. The lens is stopped down to where the spots of light due to the beamlets striking the scintillator are just visible. This insures that the spots are in the "gray zone" of the film where its response is linear. The shutter of the camera is open for a period of time longer than the duration of the shot; therefore all emittance measurements are time integrated over one shot.

To evaluate the beam emittance, we first measure the intensity profiles of the individual beamlet images as recorded on the film. The image due to each beamlet is moved (in what we will call the x-direction) across a slit which is long (in the y-direction) and thin (in the x-direction). The length of the slit in the y-direction is, in all cases, larger than the extent of the image. In this way we effectively integrate over all velocities in one transverse dimension, while determining the velocity distribution in the other transverse dimension. This velocity distribution is then appropriately weighted by the measured current density

profile of the beam and a phase space contour plot is constructed. Two such contour plots are illustrated in Fig. 4, one for a poor emittance beam, the other for our best beam. Here $\theta_x = v_x/v_z$ is plotted against x, the transverse coordinate. Finally, the emittance ϵ_0 is defined[3] as $1/\pi$ times the area in $x-\theta_x$ space of the projection of the volume in phase space that encloses 90% of the beam electrons. The normalized emittance is then given by

$$\epsilon_n = \beta\gamma\epsilon_0 \tag{1}$$

where $\beta = v/c$, v is the beam velocity, and $\gamma = (1-\beta^2)^{-1/2}$ is the energy factor related to the accelerator voltage V_0 by $\gamma = 1 + (eV_0/m_0c^2)$. Once the emittance and beam current I are determined, the normalized beam brightness[3] can be calculated from

$$B_n = I/\pi^2\epsilon_n^2 \, . \tag{2}$$

III. RESULTS

The measured emittance and beam current are found to be functions of the cathode material and the electric field at the cathode surface. We present first the results of varying the cathode material, and second the results of varying the macroscopic electric field in the cathode-anode gap.

Cathode Material.

Emittance measurements are carried out with six different cathode materials at an accelerator voltage of 2.0 MV, a cathode-anode gap spacing of 1.2 cm, and a cathode emit-

ting surface 2 cm in diameter. A summary of these measurements is presented in Table I. In the first column is the current measured by the Rogowski coil when a mesh is in place in the last anode. In the second column is the spreading angle $\delta\theta$ of the center beamlet (see Fig. 1). Here $\delta\theta$ is the half-width-at-half-maximum of the intensity profile of the center spot on the photographic film. The third column gives the measured normalized emittance, calculated using the phase space area occupied by 90% of the beam electrons as outlined in section II. The last column is the brightness calculated from Eq. 2. The measured emittances listed in Table I range from the lowest value of 83×10^{-3} (π-cm-rad) for smooth reactor graphite to the highest value of 270×10^{-3} (π-cm-rad) for smooth POCO[12] graphite.

Two photographs of the beamlet images on the ZnS scintillator screen are shown in Fig. 5. Inspection of these photographs demonstrates the dramatic differences in the beams produced from these two cathode materials. For the case of the smooth POCO graphite, the spots are large, diffuse and irregular, and the emittance is correspondingly high. For the case of the smooth reactor graphite the spots are small, round and uniform, corresponding to a lower beam emittance.

The POCO graphite is a standard commercial graphite, which is relatively hard and dense($\rho = 1.84\,\mathrm{gm/cm^3}$). The reactor graphite is a softer graphite, which is more porous and less dense ($\rho = 1.66\,\mathrm{gm/cm^3}$) than the POCO graphite. The surfaces of both materials are faced off flat and are therefore macroscopically smooth. No attempt is made to polish either surface. On a smaller scale the surface of the reactor graphite cathode is rougher due

to its greater porosity. When viewed with an electron microscope, this increased roughness extends to the microscopic scale; the graphite flakes in the POCO graphite are very ordered and lie flat on top of one another, while the graphite flakes in the reactor graphite are more randomly distributed and sharp protrusions are present. These protrusions and sharp edges on the microscopic scale produce a local electric field enhancement which may be responsible for the improved cathode turn-on and cathode plasma uniformity and therefore lower beam emittance. It is also possible that the reactor graphite has a significantly greater concentration of impurities. It has been suggested[13] that these impurities may also contribute to improved beam characteristics.

To measure the extent to which macroscopic protrusions affect emission and beam quality, concentric triangular grooves (0.5 mm deep, 0.75 mm radially separated) are cut into an otherwise smooth POCO graphite cathode. As can be seen from Table I, the result is a factor of two increase in observed current, and almost a factor of three decrease in measured emittance as compared to the smooth POCO graphite cathode. The improved beam characteristics obtained as a result of macroscopically roughening the POCO graphite cathode surface are still not as good as those obtained from a microscopically rough reactor graphite cathode.

Other cathode materials tested include sandblasted 2024 aluminum, sandblasted 2024 aluminum coated with carbon, and an epoxy inlaid POCO graphite cathode. Both the sandblasted 2024 aluminum and the carbon coated sandblasted 2024 aluminum cathodes produce beams with emittances which fall between those of the grooved POCO

graphite cathode and the smooth reactor graphite cathode. The carbon coated sand-blasted 2024 aluminum cathode produces a beam with an emittance and a current very close to those of the beam from the smooth reactor graphite cathode. Finally, the last cathode consists of smooth POCO graphite with thin concentric ribbons of epoxy filling small grooves in the surface. This configuration yields low beam current and poor emittance.

Macroscopic Electric Field In the Cathode-Anode Gap.

Variation of the macroscopic electric field strength is achieved by varying the cathode-anode gap spacing from 0.77 cm to 2.05 cm. This results in a variation of the applied electric field strength from 650 kV/cm to 245 kV/cm, respectively. For the smallest gap spacing it is necessary to use a smaller cathode diameter because our 2 cm diameter cathodes emit an excessively large current which cannot be completely focussed by the electrode structure.

The observations are summarized in Fig. 6 where we plot an effective emittance ϵ_n/r_K, the normalized emittance divided by the cathode radius, as a function of the macroscopic electric field E in the K-A gap. By normalizing the emittance in this manner we remove the effects of different cathode radii. The quantity ϵ_n/r_K is a measure of $\delta\theta$ at the cathode. Figure 6 shows that lower effective emittances are obtained at higher macroscopic electric fields. This dependence is observed for both the grooved POCO graphite and smooth reactor graphite cathodes used in the experiment. These larger macroscopic electric fields correspond to larger local microscopic electric fields at the cathode surface,

and to larger values of the rate of change of electric field dE/dt. There is evidence from other experiments[13] that increasing dE/dt results in improved cathode performance. We note that the 1 cm diameter smooth reactor graphite cathode at the 0.77 cm gap spacing produces the brightest beam, with a current of 1070 A, a normalized emittance of 38×10^{-3} (π−cm − rad), and a brightness of 74 kA/cm^{2}rad^2. The spreading angle $\delta\theta$ for the center beamlet for this case is 2.3 mrad. The phase space plot of the beam produced by this cathode is shown in Fig. 4(b).

The range of measurable emittances in this experiment is limited by the maximum acceptance angle of the aperture plate and by the minimum resolvable spot size on the film. The maximum acceptance angle is 460 mrad, which is almost an order of magnitude larger than the largest observed values of θ. The minimum resolvable $\delta\theta$ is approximately 2 mrad. Therefore, our lowest measured emittance of 38×10^{-3}(π−cm − rad) quoted above is resolution limited and represents an upper limit on the true emittance.

IV. CONCLUSIONS

We have studied the emittance characteristics of an electrostatically focussed, multistage, cold cathode electron gun. Measurements show that beam quality depends strongly on cathode material and on the strength of the applied electric field at the cathode surface. Our best results are obtained with a reactor grade graphite cathode with our highest applied electric field of 650 kV/cm. This configuration yields a normalized emittance of 38×10^{-3} (π-cm-rad) and a normalized brightness of 74 kA/cm^{2}rad^2. Our measurements

indicate that further increasing the surface electric field would most likely lead to even higher beam brightness. We note however that the maximum electric field that can be applied at the cathode is limited by the breakdown strength[9] of our anodized coating ($E \leq 900 - 1300\,\mathrm{kV/cm}$).

In Fig. 7 we plot our beam brightness along with those of beams produced in several other electron guns,[4-6,14-16] most of which find applications in free electron laser research. It has been suggested[17] that high brightness, high current electron beams can be achieved only through the use of guns immersed in strong magnetic fields ranging from approximately one kilogauss to tens of kilogauss. Figure 7 indicates that this is not necessarily the case, and that non-immersed guns can do as well (and possibly better) than immersed guns. This is a welcome conclusion. The reason for avoiding strong magnetic fields is threefold. First, strong magnetic fields occupying large volumes are often impractical. Secondly, magnetic fields cause a rippling of the beam surface. This has required experimenters[4,5,18] to remove as much as 90% of the hot outer layers, thereby reducing the overall efficiency of the free electron laser. Lastly, magnetic fields can give rise to undesirable instabilities, such as the negative mass instability,[19] the cyclotron maser instability,[20] and the diacotron instability.[21]

An important measure of beam quality[17] in a free electron laser is the fractional spread in beam axial energy $\Delta\gamma_{||}/\gamma$, where $\gamma_{||} = (1 - v_{||}^2/c^2)^{-1/2}$. A finite transverse emittance corresponds to a spread in the transverse beam velocity and therefore to a spread in $\gamma_{||}$

through the relation,[22]

$$\frac{\Delta\gamma_{\|}}{\gamma} = \frac{\epsilon_n^2}{2r_b^2} \tag{3}$$

where r_b is the beam radius. For our best beam, the axial energy spread corresponding to the measured emittance at the exit of the electron gun, where $r_b = 2.5\,\mathrm{cm}$, is $\Delta\gamma_{\|}/\gamma = 1.2 \times 10^{-4}$.

The ultimate emittance $\epsilon_n(\mathrm{thermal})$ is one in which the electron temperature at the cathode surface T_K is the limiting parameter. Under these conditions,[23]

$$\epsilon_n(\mathrm{thermal}) \simeq 2r_K\left(\frac{\kappa T_K}{m_0c^2}\right)^{1/2} \tag{4}$$

where r_K is the cathode radius. Assuming that for a cold cathode the emitted electrons are in thermal equilibrium with the underlying plasma where the temperature is typically in the range[13] $3 - 10\,\mathrm{eV}$, one finds from Eq. (4) that $\epsilon_n(\mathrm{thermal}) \simeq (5-9) \times 10^{-3} r_K$ (π-cm-rad). For our 1 cm diameter cathode cited above, the corresponding beam brightness would be in the range $B_n(\mathrm{thermal}) \simeq (0.4 - 1.6) \times 10^4\,\mathrm{kA/cm^2rad^2}$, which exceeds our best result by about two orders of magnitude.

One may also wish to compare the present result with the brightness obtained from the empirical Lawson-Penner condition often used to characterize beams produced by thermionic electron guns, namely,

$$\begin{aligned} \epsilon_n(L-P) &\simeq 0.3[I(\mathrm{kA})]^{1/2} \quad (\pi\mathrm{-cm-rad}) \\ B_n(L-P) &\simeq 1.1 \quad \mathrm{kA/cm^2rad^2} \end{aligned} \tag{5}$$

From this we see that the brightness of our beam is nearly two orders of magnitude greater than $B_n(L-P)$.

ACKNOWLEDGEMENTS

This work is supported in part by the Air Force Office of Scientific Research, in part by the National Science Foundation, and in part by the Lawrence Livermore National Laboratory. One of us (G.B.) also gratefully acknowledges help in gun design provided by Dr. H.B. Schilling.

REFERENCES

1. P.A. Sprangle, R.A. Smith, and V.L. Granatstein, in "Infrared and Submillimeter Waves", ed. K. Button,(New York: Academic Press, 1980), Vol. 1, p.279 and references therein.

2. T.J. Kwan and C.M. Snell, Phys. Fluids **26**, 835 (1983).

3. C. Lejeune, and J. Aubert, in "Applied Charged Particle Optics", ed. A. Septier, (Academic Press), Part A, p.159 - 259 (1980).

4. R.H. Jackson, S.H. Gold, R.K. Parker, H.P. Freund, P.C. Efthimion, V.L. Granatstein, M. Herndon, A.K. Kinkead and J.E. Kosakowski, IEEE J. of Quantum Electron., **QE-19**, 346, (1983).

5. M.L. Sloan and H.A. Davis, Phys. Fluids **25**, 2337 (1982).

6. G.J. Caporaso. W.A. Barletta, D.L. Birx, R.J. Briggs, Y.P. Chong, A.G. Cole, T.J. Fessenden. R.E. Hester, E.J. Lauer, V.K. Neil, A.C. Paul, D.S. Prono, and K.W. Struve, Proc. of the Fifth Int. Conf. on High-Power Particle Beams, p.427 (1983); T.J. Fessenden. Lawrence Livermore National Laboratory Report UCID-19839 (1983).

7. R.L. Sheffield, M.D. Montgomery, J.V. Parker, K.B. Riepe, and S. Singer, J. Appl. Phys., **53**, 5408 (1982).

8. M.E. Jones and L.E. Thode, J. Appl. Phys. **51**, 5212 (1980); M.E. Jones, M.A. Mostrom, and L.E. Thode, J. Appl. Phys. **52**, 4942 (1981); M.A. Mostrom, M.E. Jones, and L.E. Thode, J. Appl. Phys. **52**, 1266 (1981).

9. J. Fink, H.B. Schilling, and V. Schumacher, J. Appl. Phys., **51**, 2995 (1980).

10. W. Dommaschk, Max-Plank-Institut Für Plasmaphysik, Garching bei München, **IPP 0/12**, (1973).

11. B. Kulke and R. Kihara, Lawrence Livermore Laboratory Preprint UCRL-82533 (1979); J.G. Kelly and L.P. Bradley, Sandia National Laboratory Report SC-RR-72 0058 (1972).

12. POCO graphite is manufactured by UNION-76 Inc. The graphite used in this experiment is specified as type AXF-5Q.

13. D.D. Hinshelwood, IEEE Trans. on Plasma Sc., **PS-11**, 188 (1983); and D.D. Hinshelwood. Ph.D. thesis, Department of Physics, Massachusetts Institute of Technology, 1984 (unpublished).

14. L. Elias and G. Ramian, U. Cal. at Santa Barbara Report QIFEL18/83 (1983).

15. J. Fajans, G. Bekefi, Y.Z. Yin, and B. Lax, Phys. Rev. Lett. **52**, 246 (1984).

16. J.A. Pasour, private communication.

17. C.W. Roberson, Proc. of Soc. of Photo-Optical Intr. Eng., **453**, 320 (1983).

18. R.E. Shefer and G. Bekefi, Appl. Phys. Lett. **37**, 901 (1980).

19. Y.Y. Lau and D. Chernin, Phys. Rev. Lett. **52**, 1425 (1984), and references therein.

20. P. Sprangle and A.T. Drobot, IEEE Trans. Microwave Theory Tech. **25**, 528 (1977), and references therein.

21. R.C. Davidson, "Theory of Nonneutral Plasmas", (W.A. Benjamin), p.66-78 (1974).

22. V.K. Neil, Jason Technical Report JSR-79-10 (1979).

23. J.D. Lawson, "The Physics of Charged Particle Beams", (Oxford University Press), p.201 (1977).

24. The brightness plotted for the NRL(VEBA) beam is obtained from reference [4] using the emittance calculated from the average quoted value of $\beta_\perp$. The error bars reflect the upper and lower bounds on the brightness calculated from the quoted upper and lower bounds on $\beta_\perp$.

Table I.

Current and Emittance as a Function of Cathode Material

V = 2.0 MV, K − A gap = 1.20 cm, 2 cm diameter emitting surface.

Cathode Material	Current (Amps)	$\delta\theta$ (mrad)	Emittance $(\times 10^{-3}\,(\pi\text{−cm} - \text{rad}))$	Brightness $(\text{kA/cm}^2\text{rad}^2)$
Smooth POCO Graphite	750	18	270	1.0
Epoxy Inlaid Grooved POCO Graphite	930	8.9	180	2.9
Sandblasted 2024 Al	1300	5.2	104	12
Grooved POCO Graphite	1490	5.5	110	13
Carbon Coated Sandblasted 2024 Al	1610	4.2	86	22
Smooth Reactor Graphite	1660	4.2	83	24

Figure Captions

Fig. 1. Experimental arrangement (upper) and detail of emittance diagnostic (lower).

Fig. 2. Longitudinal cross-section of five stage multi-electrode gun.

Fig. 3. Oscilloscope traces of voltage on the electron gun (upper) and beam current (lower). The peak values are V = 2.0 MV and I = 1.1 kA.

Fig. 4. Phase space contour plots for beams produced at (a) a smooth POCO graphite cathode and (b) a smooth reactor graphite cathode. In both cases we show the contours of constant phase space density which enclose 90% of the beam electrons.

Fig. 5. Beamlet images on the ZnS scintillator screen for beams produced at (a) a smooth POCO graphite cathode and (b) a smooth reactor graphite cathode. In both cases V = 2.0 MV, the K-A gap spacing is 1.2 cm and the cathode diameter is 2.0 cm.

Fig. 6. Effective emittance ϵ_n/r_K vs applied electric field E in the cathode-anode gap for two different cathode materials.

Fig. 7. Electron beam brightnesses and beam currents measured in other experiments compared with those measured in this experiment (MIT-B). The circles represent electron guns immersed in strong magnetic fields ($B > 1$ kG), and the triangles represent non-immersed guns. The listed experiments UCSB[14] and MIT-A[15] use thermionic

cathodes. The experiments ARA[5], ATA[6], NRL[16], NRL(VEBA)[24], and MIT-B use cold cathodes.

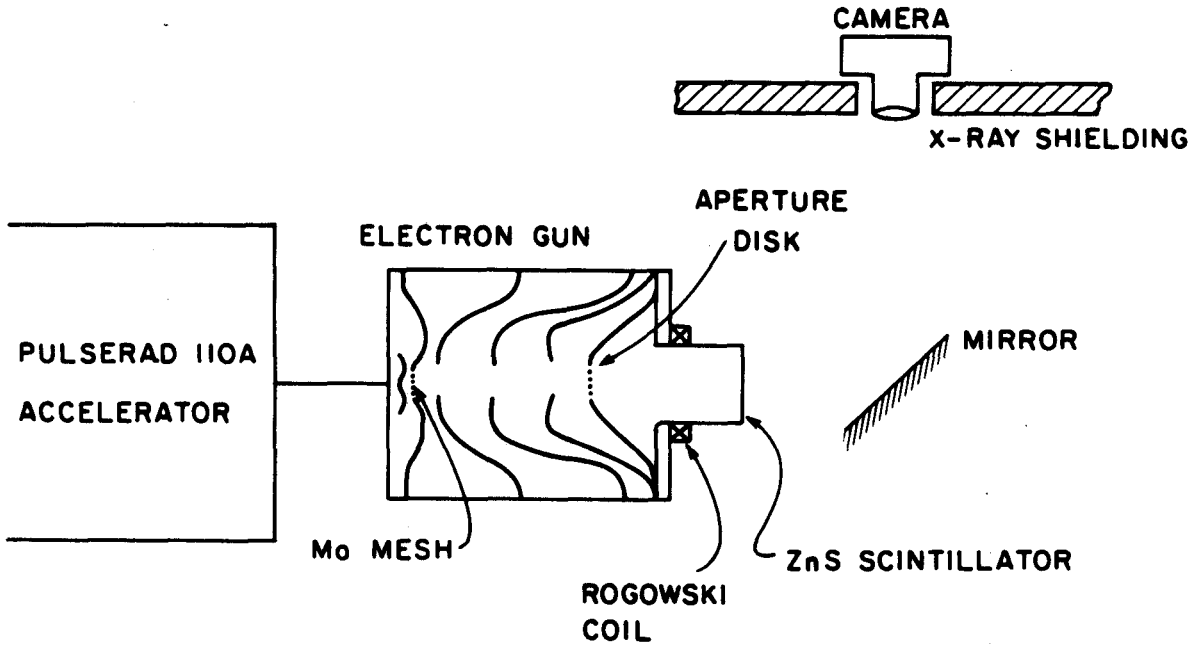

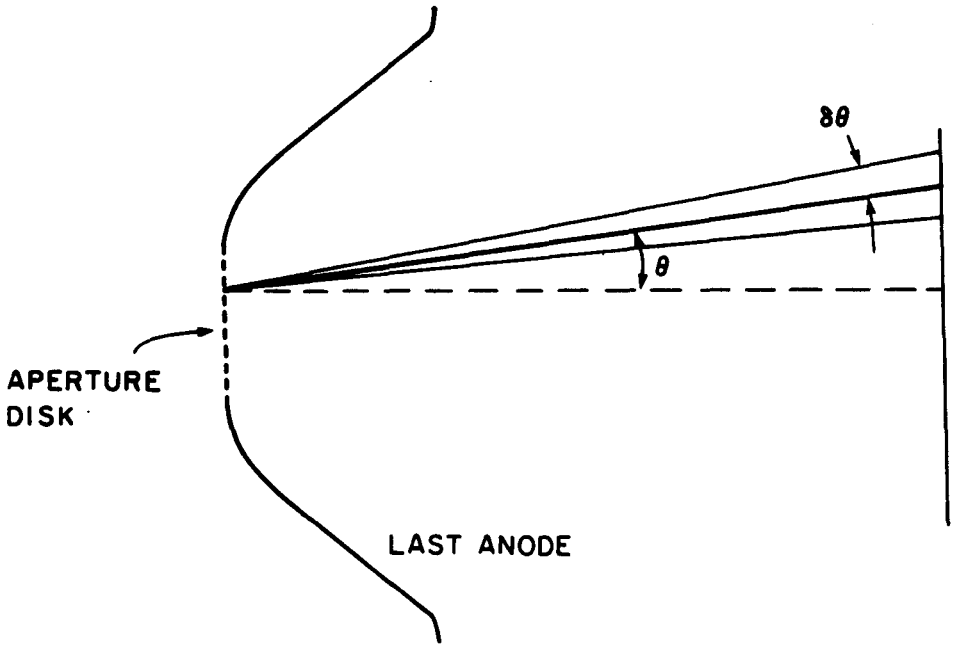

Fig. 1
Kirkpatrick, Shefer, Bekefi

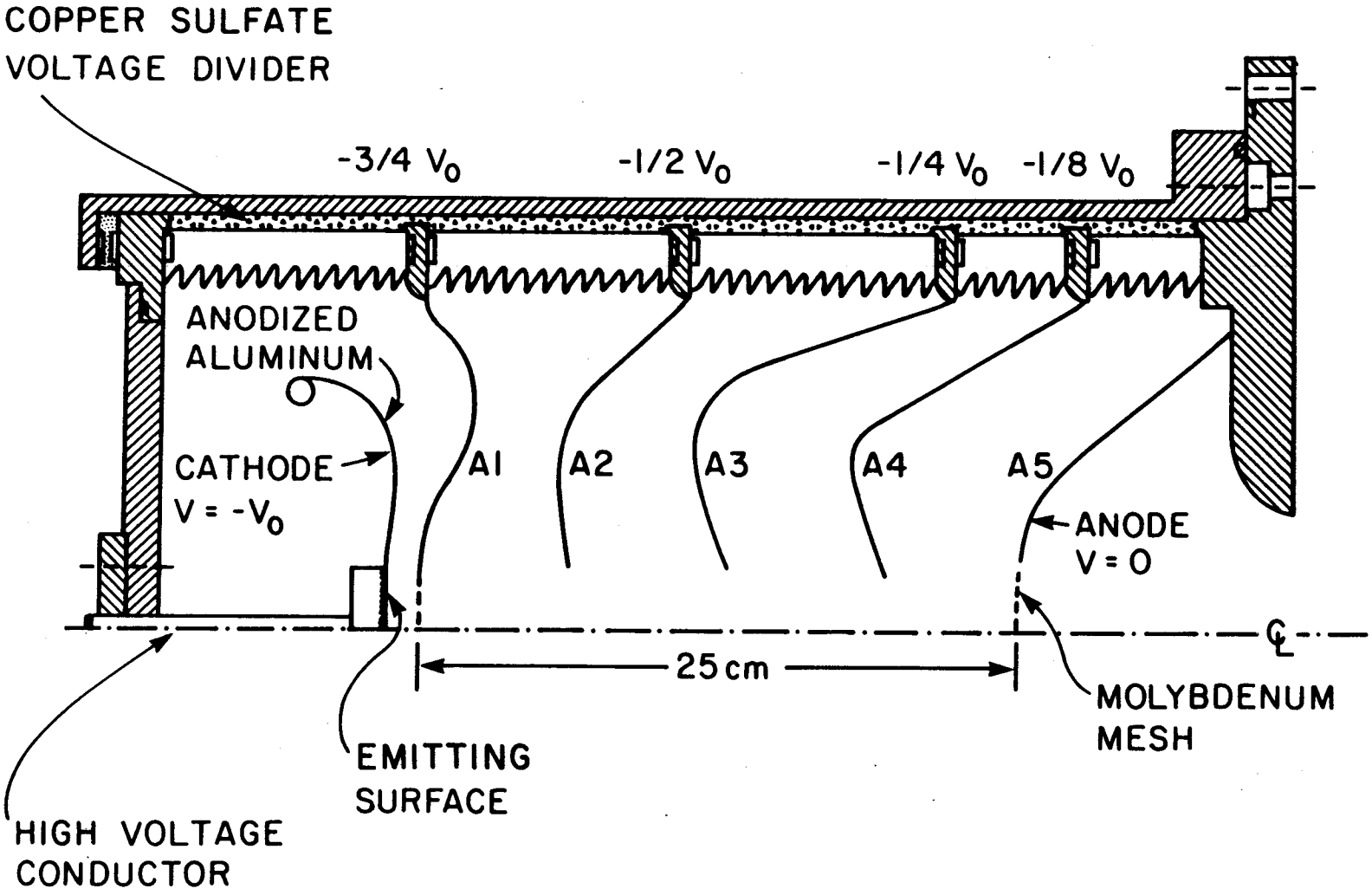

Fig. 2
Kirkpatrick, Shefer, Bekefi

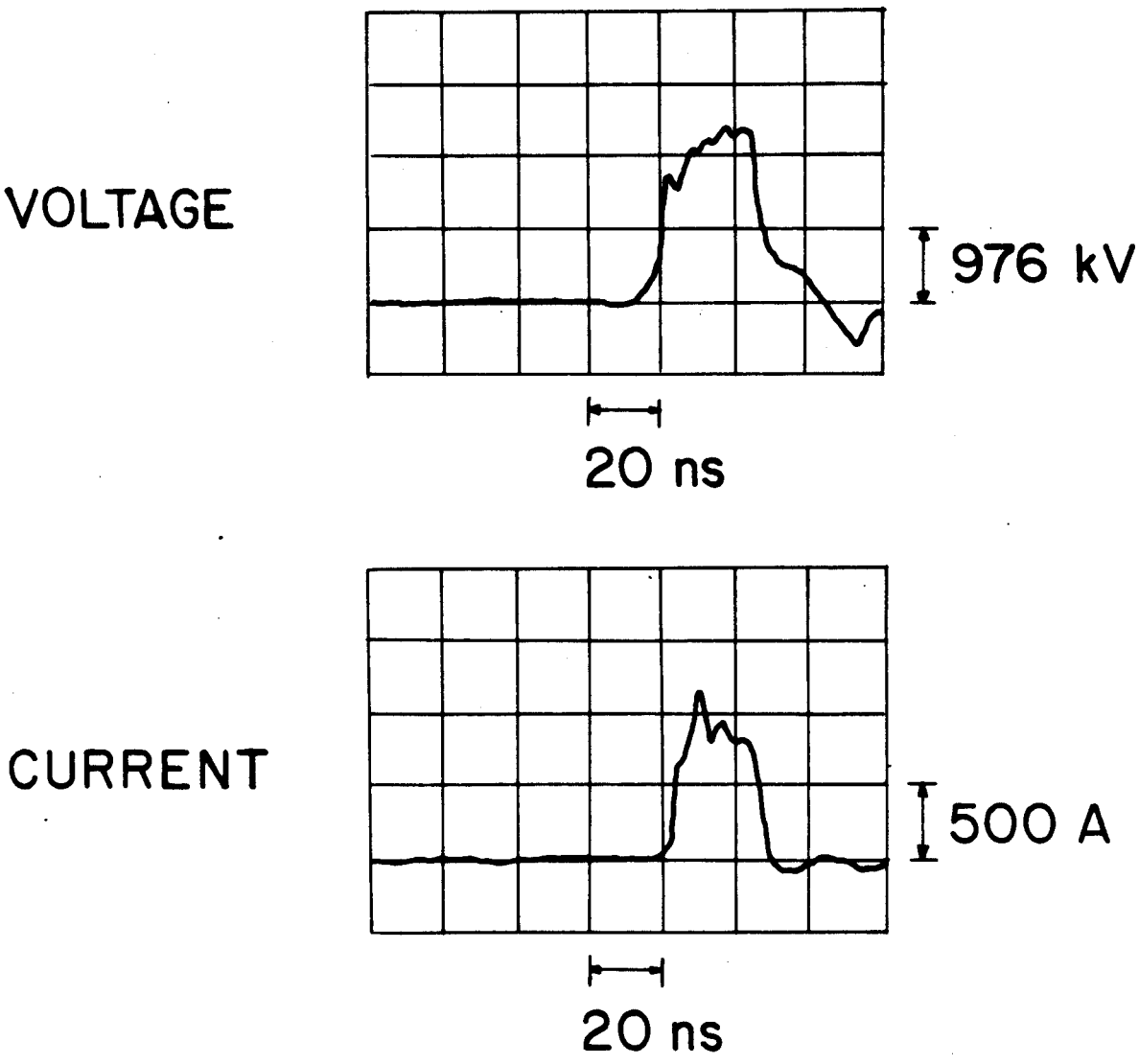

Fig. 3
Kirkpatrick, Shefer, Bekefi

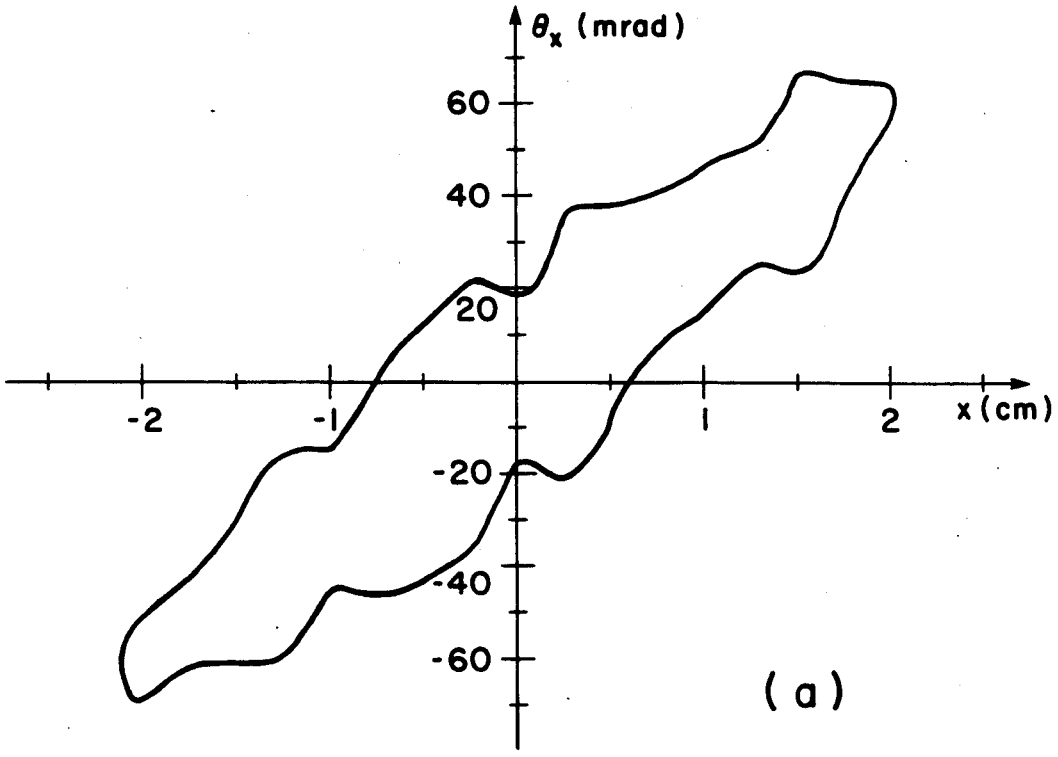

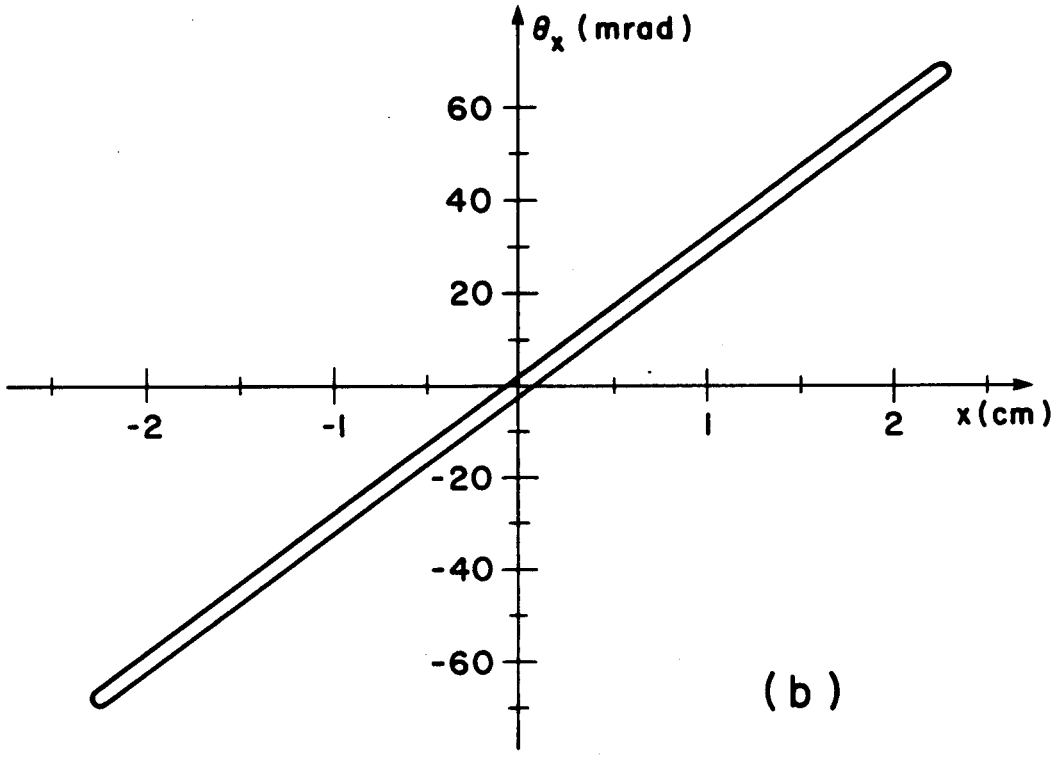

Fig. 4
Kirkpatrick, Shefer, Bekefi

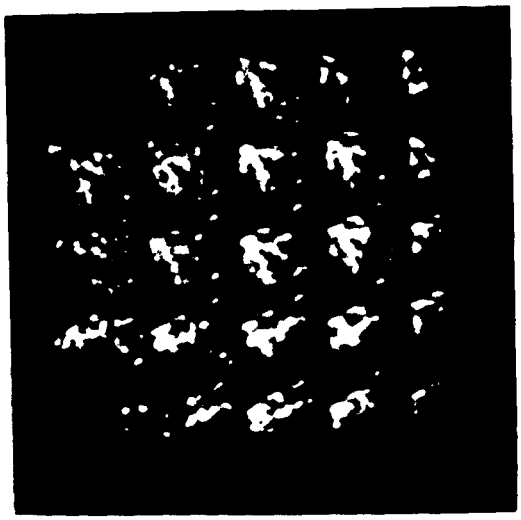

(a)

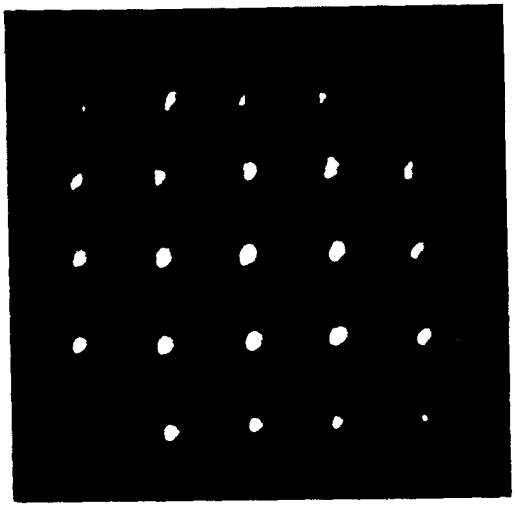

(b)

Fig. 5
Kirkpatrick, Shefer, Bekefi

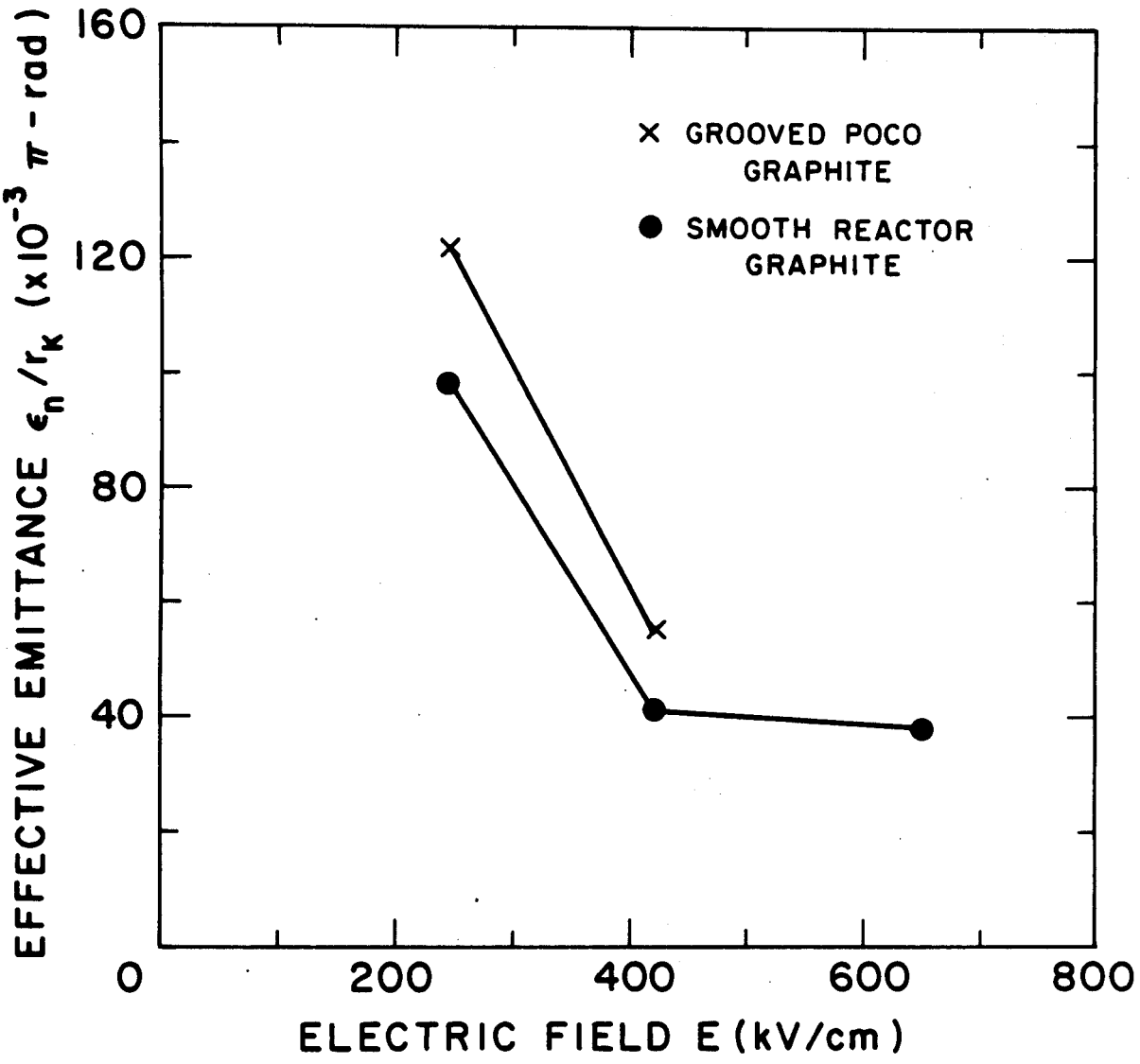

Fig. 6
Kirkpatrick, Shefer, Bekefi

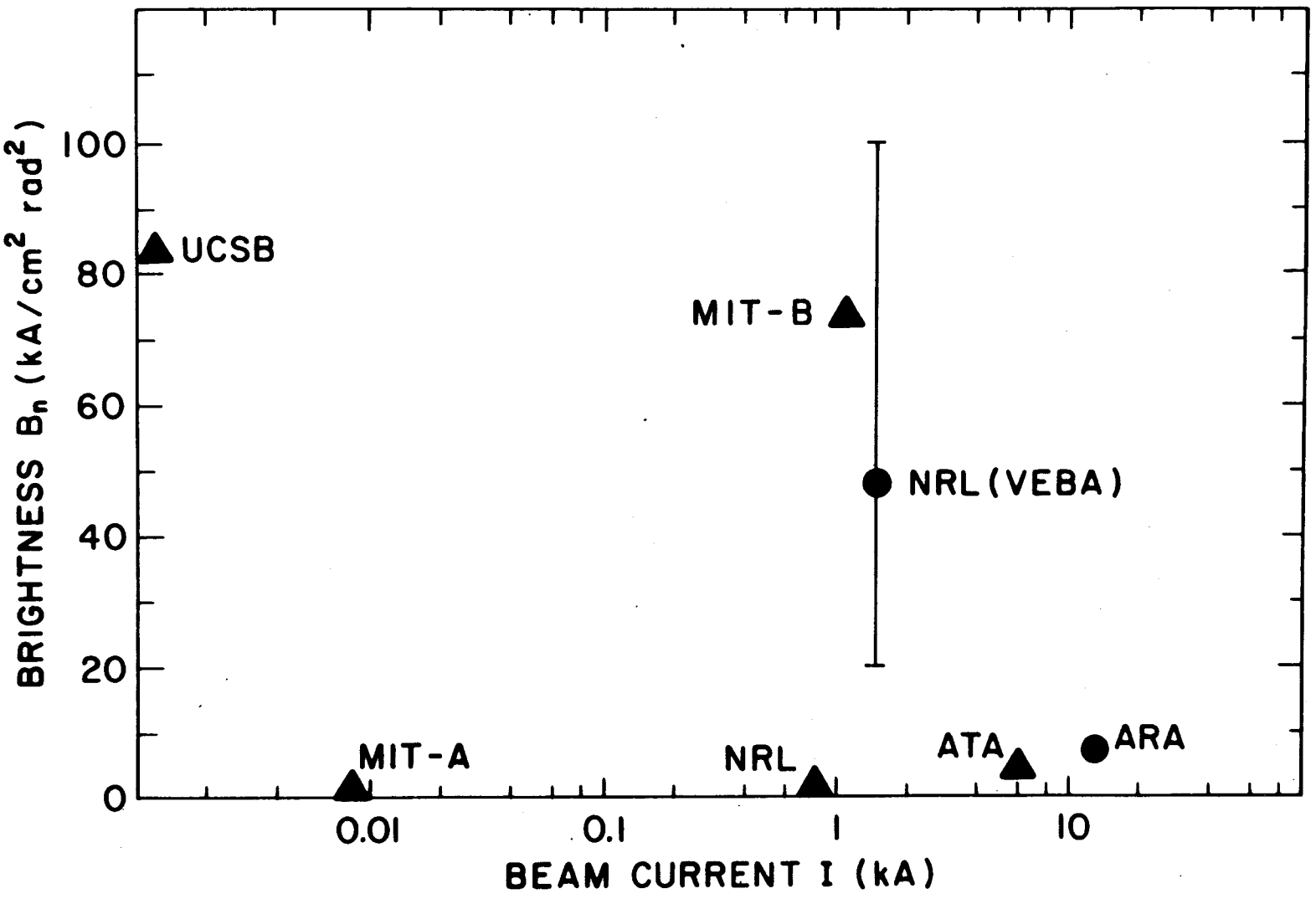

Fig. 7
Kirkpatrick, Shefer, Bekefi